Inner Structure of Thin Films of Lamellar Poly(styrene-*b*-butadiene) Diblock Copolymers As Revealed by Grazing-Incidence Small-Angle Scattering

P. Busch,[†,#] D. Posselt,[§] D.-M. Smilgies,[‡] M. Rauscher,[||] and C. M. Papadakis*,[⊥,†]

Faculty of Physics and Earth Sciences, University of Leipzig, Linnéstr. 5, D-04103 Leipzig, Germany; Cornell High Energy Synchrotron Source (CHESS), Wilson Laboratory, Cornell University, Ithaca, New York 14853; Department of Mathematics and Physics (IMFUFA), Roskilde University, P.O. Box 260, DK-4000 Roskilde, Denmark; Max-Planck-Institute for Metals Research, Heisenbergstr. 3 and Institute of Theoretical and Applied Physics, Universität Stuttgart, Pfaffenwaldring 57/VI, D-70569 Stuttgart, Germany; and Physikdepartment E13, Technische Universität München, James-Franck-Str. 1, D-85747 Garching, Germany

Received July 26, 2006; Revised Manuscript Received November 3, 2006

ABSTRACT: The lamellar orientation in supported, thin films of poly(styrene-*b*-butadiene) (P(S-*b*-B)) depends on block copolymer molar mass. We have studied films from nine block copolymer samples with molar masses between 13.9 and 183 kg/mol using grazing-incidence small-angle X-ray scattering (GISAXS) and have found that in low molar mass samples the lamellae are parallel to the substrate surface, whereas they are perpendicular for high molar masses. For a thick, high molar mass film, the bulk limit is approached; i.e., randomly oriented lamellae are present. The 2D GISAXS images are discussed quantitatively in the framework of our recently developed distorted-wave Born approximation model (Busch, P.; et al. *J. Appl. Crystallogr.* **2006**, *39*, 433). The results cannot be explained from enthalpic considerations alone but point to the importance of entropic factors.

Introduction

Diblock copolymer thin films are prominent candidates for a range of applications requiring nanostructured surfaces, such as the creation of nanoporous films and of arrays of nanowires as well as their use as photonic crystals and biosensors (for recent reviews see refs 1−3). Because of the repulsion between two interconnected, chemically dissimilar blocks, they are able to undergo self-organization into regular nanostructures on the length scale of 10−100 nm. This "bottom-up" approach allows for the creation of large patterns in a more efficient way than traditional lithographic ("top-down") techniques.[4] The diblock copolymer nanostructure in the ordered phase is controlled by a number of parameters, such as the interaction energy between the two blocks, the relative size of the two blocks, and the overall degree of polymerization, i.e., molar mass. In theoretical work on thin films, the interface enthalpies and entropies at the air−polymer and the polymer−substrate interface,[5−7] the roughness of the substrate,[8] and confinement effects[9] enter as additional parameters. In a previous publication, we have shown that molar mass can be the determining parameter regarding the orientation of the nanostructure relative to the film surface for thin films of lamellar poly(styrene-*b*-butadiene) (P(S-*b*-B)).[10] Using atomic force microscopy (AFM), we have found that in low molar mass (below ∼ 55 kg/mol) P(S-*b*-B) films the lamellae form terraces at the film surface, which is characteristic for a parallel orientation near the film surface, while for high molar masses (above ∼90 kg/mol) the lamellae are perpendicular to the surface. For intermediate molar masses, surface topographies inconsistent with both the parallel and the perpendicular orientation were found. We thus suggested a morphology, where different orientations coexist.

However, AFM only reveals the surface texture of the film, and our results were therefore substantiated by referring to grazing-incidence small-angle X-ray scattering (GISAXS) studies of the corresponding films. GISAXS offers a unique, noninvasive method to obtain information on both lateral and transverse structures inside thin films. Examples are the dewetting of diblock copolymer films,[11−14] the lamellar orientation of symmetric diblock copolymer films and its changes in solvent vapor,[15,16] the ordering of a cylindrical block copolymer morphology during evaporation of solvent,[17] and the structures of films in the hexagonal, the gyroid, or the hexagonally perforated layer phase.[18,19] A certain degree of depth resolution can be obtained by varying the angle of incidence of the X-ray beam and thus the penetration depth.

A brief overview of the results from our AFM and GISAXS studies has been given in ref 20 with the focus on the advantages of the GISAXS method. In the present report, the results of our GISAXS experiments from lamellar P(S-*b*-B) thin films of a large range of molar masses are discussed in detail with the focus on the prevailing lamellar orientation in the film as well as the lateral and vertical sizes of the lamellar domains. For films with a meandering surface pattern indicative of perpendicular lamellae, GISAXS has been used to clarify whether the perpendicular orientation prevails throughout the entire film. Other films display terraces at the film surface, which are characteristic for a parallel orientation of the lamellae. However, the terrace height was not always identical to the bulk lamellar thickness, and by means of GISAXS the parallel orientation could be verified or lamellae having other orientations could be detected. For each molar mass, the film thickness has been varied, allowing us to determine when the bulk limit is reached, i.e., which film thickness is required in order to lose the

* Corresponding author. E-mail: cpapadak@ph.tum.de.
[†] University of Leipzig.
[‡] Cornell University.
[§] Roskilde University.
[||] Universität Stuttgart.
[⊥] Technische Universität München.
[#] Present address: JCNS-FRMII, TU München, Lichtenbergstr. 1, 85747 Garching, Germany.

10.1021/ma061695c CCC: $37.00
Published on Web 01/05/2007

influence of the air−polymer and the polymer−substrate interface regarding the orientation of the lamellae, resulting in a completely random orientation of lamellar domains in the center of the film.[21] In some cases, the interpretation of our AFM data was difficult, and the application of GISAXS helped to clarify whether any internal ordering of the film remained. Our analysis is based on the GISAXS scattering cross section for thin lamellar films which we have calculated in the distorted-wave Born approximation (DWBA).[22]

Experimental Section

The poly(styrene-*b*-butadiene) (P(S-*b*-B)) diblock copolymers used in this study were synthesized by anionic polymerization.[23] The samples have number-average molar masses between 13.9 and 183 kg/mol, a polybutadiene (PB) volume fraction of 0.49 ± 0.01, and polydispersity indices below 1.1.[24] Their bulk lamellar thicknesses, D_{lam}^{b}, increase with molar mass and range between 138 and 839 Å.[24,25] The Flory−Huggins segment−segment interaction parameter is $\chi = A/T + B$ with $A = 21.6 \pm 2.1$ K and $B = -0.019 \pm 0.005$, as determined from the order−disorder transition temperatures.[25] The glass transition temperatures of the polystyrene (PS) blocks lie between 76 and ∼102 °C,[25] whereas that of the polybutadiene (PB) homopolymer is below −80 °C.[26] The surface tensions of PS and PB are $\gamma_c^{PS} = 33$ mN/m and $\gamma_c^{PB} = 28$ mN/m, respectively.[27]

Thin films were prepared on Si(111) wafers terminated with a native silicon oxide layer (Silchem Handelgesellschaft mbH). The cleaning procedure is described in ref 10. The polymers were dissolved in toluene together with ∼1% w/w (relative to the polymer mass) antioxidant (Irganox 1010 from CIBA) to prevent cross-linking of the PB blocks during further treatment. Solutions with polymer concentrations between 0.1% and 7% w/w were poured onto the Si wafers until these were completely wet, and films were spin-coated at 3000 rpm for 30 s. To remove traces of solvent and to drive the films toward equilibrium, the films were dried in high vacuum (∼10^{-5} mbar) for up to 3 days. For films with $\bar{M}_n \geq 54.5$ kg/mol, drying was performed at 150 °C, i.e., well above both glass transition temperatures but still in the lamellar state. Films with lower molar masses were dried at room temperature to avoid dewetting. The film thicknesses were determined using standard spectroscopic ellipsometry (see ref 10).

Scattering experiments were performed at D-line at the Cornell High Energy Synchrotron Source (CHESS) at Cornell University in Ithaca, NY, at ID10B at the European Synchrotron Radiation Facility (ESRF) in Grenoble, France, and at BW4, HASYLAB at DESY in Hamburg, Germany. The schematics of the GISAXS experiment are shown in Figure 1. At D-line and at ID10B beamlines, an X-ray beam with a wavelength $\lambda = 1.54$ Å was used. Bandwidth at D-line was 1.5% (multilayer optics) and 10^{-5} at ID10B (diamond (111) monochromator). The beam was collimated by two collimation slits and a guard slit, and the horizontal beam width was 0.5 mm. In order to keep the footprint of the beam along the sample smaller than the sample length of 40 mm at incident angles of ∼0.2°, the vertical width of the beam was reduced to 50 μm. At BW4, the wavelength was 1.38 Å with a bandwidth of 10^{-4} (Si(111) monochromator), and the beam was focused by Be lenses to a size of 78×46 μm^2 (horizontal × vertical) at the sample position, which limits the footprint to 13 mm at an incident angle of 0.2°. A molybdenum rod with a diameter of 1.25 mm (D-line and ID10B) or 1.5 mm (BW4) served as a beamstop for the intense reflected beam and the strong diffuse scattering in the incident plane. CCD cameras with a dynamic range of 3 decades were used for the detection of the scattered intensity at all beamlines. The pixel sizes were 22.5 μm at ID10B, 50.8 μm at D-line, and 79.1 μm at BW4. With the setup described, it is possible to resolve lateral structures of up to 1000 Å at a sample−detector distance of typically 1 m. In order to minimize radiation damage, the sample was moved sideways after alignment, so that a pristine sample spot was exposed to the beam during the GISAXS measurements. $q_{||} = \sqrt{q_x^2 + q_y^2}$ and q_z are the in-plane and the normal components of the scattering vector, respectively. For small incident and scattering angles, the coordinates of our 2D detector correspond approximately to q_y and to q_z.

GISAXS images were recorded with exposure times of 10 s (unless stated otherwise) and were corrected for background from dark current and read-out noise. Flat-field corrections were applied at D-line as well as distortion corrections for the fiber-coupled CCD camera used at CHESS.[28] In the 2D maps shown, the pixels were binned 2×2 for the clarity of presentation. Intensity profiles along q_y were obtained by taking a single pixel row. Intensity profiles along q_z were obtained by integrating along q_y between −0.005 and 0.005 Å^{-1}. The positions and the widths of the peaks in the profiles were determined by fitting Lorentzians on a linear background. The uncertainties of the positions amount to ∼2×10^{-4} Å^{-1}, unless stated otherwise.

At D-line, the zero of the incident angle was adjusted with a precision of 0.02° before the measurements by determining the onset of the X-ray reflectivity curve using an ion chamber. Refined incident angles were determined afterward from the q_z position of the specular peak in the 2D GISAXS image.

The transversal coherence lengths of the beam are large compared to typical domain sizes observed in AFM but small compared to the illuminated area, such that accurate statistical averages are obtained. The films scatter coherently over their entire thickness.[22]

In spite of the differences of the various instruments used, the results are consistent. Certain features are common to all the GISAXS maps: (i) The direct beam was not observed, since it is too intense for the detector and had to be blocked by a blade. (ii) For a specific GISAXS map, the incoming angle of the beam, α_i, is fixed, and the (very intense) specularly reflected beam appears at an exit angle, α_f, equal to α_i; however, the specular beam is blocked with a rodlike beamstop (which leads to as a stripe of low intensity around $q_y = 0$), and only its wings are observed on each side of the beamstop. This beamstop blocks also the intense diffuse scattering in the incident plane. (iii) The maps display enhanced scattering intensity (Yoneda peaks) at exit angles corresponding to the critical angles of total external reflection from P(S-*b*-B) ($\alpha_{cP} = 0.15°$) and of SiO_x ($\alpha_{cS} = 0.22°$) (ref 29, at an X-ray energy of 8 keV).[22] Between the film and the substrate Yoneda peaks, other dynamic features may show up, depending on the contrast and the quality of the film.

Analysis of the GISAXS Maps. The GISAXS maps presented below have been analyzed in the framework of a DWBA approach described in detail in our previous publication.[22] The aspects important for the interpretation of our data in this paper are the following: The lamellar block copolymer film is considered to be the sum of a homogeneous, flat film on a planar substrate and the internal, lamellar film structure which can be treated as a perturbation. The advantage of this approach is that the scattering of the homogeneous, flat film can be calculated analytically, whereas the lamellar structure (parallel or perpendicular) can be treated in a first-order perturbation theory. The refraction of the incident beam at the surface of the polymer film and the reflection of the incident and/or the scattered beam at the film/substrate interface are taken into account when calculating the scattering cross section in the distorted-wave Born approximation.

For the *perpendicular* lamellar orientation, the differential scattering cross section for diffuse scattering factorizes into two terms: $d\sigma/d\Omega = g(\mathbf{q}_{||})|f(k_{iz},k_{fz},D_{film})|^2$. The first factor, $g(\mathbf{q}_{||})$, is the Fourier transform of the density−density correlation function, which only depends on the components of the scattering vector in the film plane, $\mathbf{q}_{||} = (q_x, q_y)$. The two-dimensional lamellar structure gives rise to constructive interference at multiples of $q_{||} = 2\pi/D_{lam}^{f}$, where D_{lam}^{f} denotes the lamellar thickness (i.e., the repeat distance) in the film. The intensity profile along the *z*-component of the momentum transfer, q_z, is described by the second factor. The momentum transfer normal to the sample plane is $q_z = k_{fz} - k_{iz}$ with $k_{iz} = (4\pi \sin \alpha_i)/\lambda$ and $k_{fz} = (4\pi \sin \alpha_f)/\lambda$ being the *z*-components of the incident and the exit wave vector. For fixed k_{iz}, i.e., in a specific GISAXS map, each value of k_{fz} corresponds

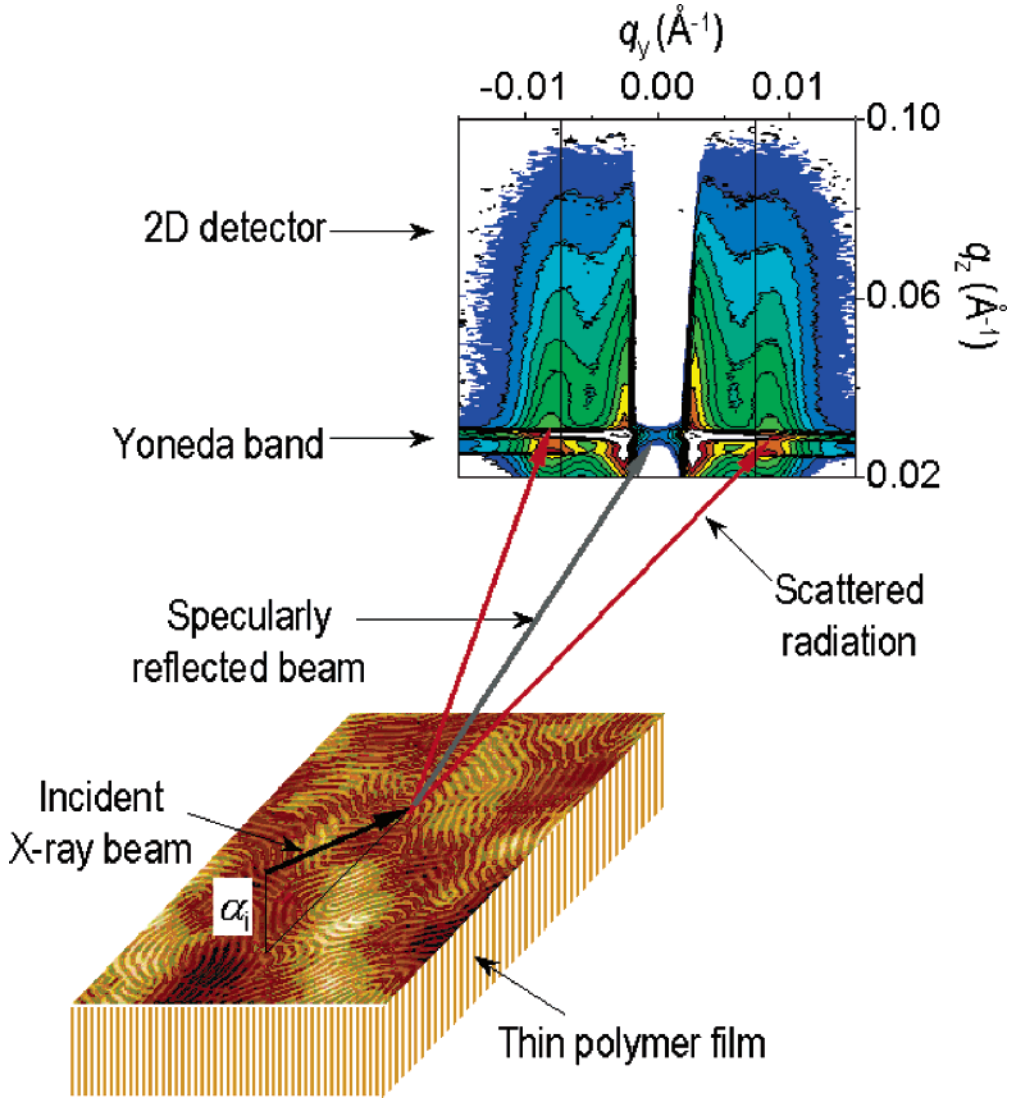

Figure 1. Schematic drawing of the experimental GISAXS setup for the case of a film with perpendicular lamellae. The beam propagates in the *x*-direction and the film normal is along the *z*-direction, while the measured $\mathbf{q}_{||}$ is along the *y*-direction. α_i is the angle of incidence, typically chosen between 0.1° and 0.3°, thus in the vicinity of the critical angles of the polymer film and the substrate. The intensity is monitored on a two-dimensional detector in the $y-z$ plane. The detector is protected from the specularly reflected beam by a rodlike beamstop. The incident beam penetrates the whole film above the critical angle of the polymer film and is scattered by the lamellar structure in the film which gives rise to Bragg rods in the case of perpendicular lamellae, indicated by vertical lines.

to a certain value of q_z. $|f(k_{iz},k_{fz},D_{film})|^2$ is modulated in a characteristic way: Above α_{cS}, fringes are observed which have a period related to the film thickness, D_{film} (see Figure 4b in ref 22). They may, however, be smeared out for films with an inhomogeneous thickness. In summary, in the two-dimensional GISAXS maps of laterally ordered films, interference peaks (Bragg rods) are expected at parallel momentum transfers being a multiple of $2\pi/D^f_{lam}$ and with a q_z-profile mainly being a function of D_{film}. A typical GISAXS map for the case of perpendicular lamellae is shown in Figure 1.

A lamellar diblock copolymer film with the lamellae *parallel* to the substrate surface can be viewed as a multilayer system of alternating polystyrene and polybutadiene layers. Flat lamellae give rise to interference peaks at distinct positions along the q_z-axis in the plane of incidence, i.e., for $q_{||} = 0$. Correlated roughness of the layers with a wavelength smaller than the lateral coherence length leads to widening of the peaks along $q_{||}$, leading to the so-called diffuse Bragg sheets, which can be observed close to the rodlike beamstop. For polymer films with weak internal contrast, it is appropriate to neglect refraction at the internal lamellar interfaces. This is the case for P(S-*b*-B) because the electron densities of PS and PB only differ by 13%. The q_z-positions of the lamellar diffraction peaks appearing in addition to the specularly reflected beam and the Yoneda peaks of the polymer film and the substrate are given by

$$q_z = \frac{2\pi}{\lambda}\left(\sin\alpha_i + \sqrt{\sin^2\alpha_{cP} + \left[\frac{m\lambda}{D^f_{lam}} \pm \sqrt{\sin^2\alpha_i - \sin^2\alpha_{cP}}\right]^2}\right) \quad (1)$$

where *m* is a positive, odd integer in the case of symmetric lamellae. Note that for eq 1 the refraction of the incoming and outgoing X-ray beams at the air−film interface was properly accounted for. The two branches of this curve correspond to the Bragg diffraction of the reflected beam (upper branch) and the direct diffraction process, which merges with the process where the diffracted beam is reflected from the substrate (lower branch) (see ref 22). The equation holds for the reflection geometry used in our GISAXS experiments, where both α_i and α_f are positive. Roughness of the layers on a length scale larger than the transversal coherence length can be viewed as the coexistence of domains with different orientations and results in bending of the diffuse Bragg sheets. This scattering feature can also be interpreted as a partial powder ring.

Results

In our previous AFM study of the surface texture of thin films of lamellar P(S-*b*-B) samples, we have found an unexpected

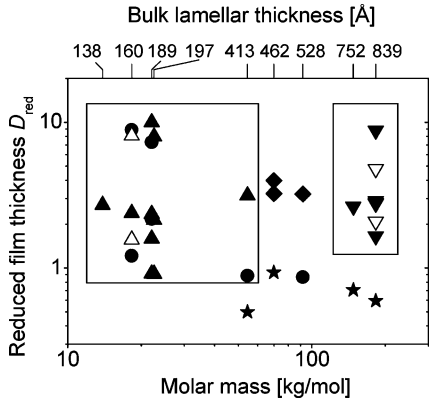

Figure 2. Orientation diagram of the surface texture as found using AFM.[10] The orientations are given as a function of block copolymer molar mass (bottom axis) or bulk lamellar thickness (top axis, values from ref 25) and of the reduced film thickness. Triangles up: parallel; triangles down: perpendicular; diamonds: coexisting orientations; stars: weak surface texture; circles: no surface texture. Filled symbols: spin-coated samples; open symbols: solvent-cast samples.

molar mass dependence of the lamellar orientation as described in the Introduction.[10] The lamellar orientation was found to be independent of the reduced film thickness, D_{red}, in the range of ~1−10 for a number of samples (the reduced film thickness is defined as $D_{red} = D_{film}/D^b_{lam}$). The lamellar orientations deduced from the surface textures of all films are compiled in Figure 2. In a few cases, especially for intermediate molar masses, the surface textures could not be attributed to a specific lamellar orientation because the surface shows neither terraces nor a clear lamellar texture.

In order to elucidate the inner film structures and to relate them to the surface textures observed, we have performed GISAXS experiments on samples identical or similar to the ones studied with AFM. Accordingly, the samples have been studied as a function of molar mass and (reduced) film thickness. In the following, we present the GISAXS results from low, intermediate, and high molar mass films and describe how the lamellar orientation in the films is determined from a qualitative analysis of the GISAXS maps. A quantitative analysis of the lamellar structures using the recently developed DWBA model is carried out.[22] Finally, the orientation diagram inside the films and the mechanisms of structure formation during film formation are discussed.

Low Molar Mass Regime. The AFM images of thin films of P(S-*b*-B) diblock copolymers with molar masses between 13.9 and 54.4 kg/mol show in many cases terraces at the film surface with terrace heights equal to D^b_{lam} within 10−20%, but consistently with a lower value.[20] The occurrence of such terraces is due to the incommensurability between D_{film} and D^b_{lam} leading to the formation of an incomplete top layer with a height similar to the bulk lamellar thickness. Terraces are thus indicative of a parallel lamellar orientation and have frequently been observed on systems chemically different from the one studied here.[30−34]

We present a relatively thick film first. Figure 3a shows the GISAXS map of a film with a block copolymer molar mass of 22.6 kg/mol and $D_{red} = 8.0$. The GISAXS map does not show any peaks at $q_y = \pm 2\pi/D^b_{lam}$; i.e., the film does not contain a noticeable amount of perpendicular lamellae. Instead, near $q_y = 0$, peaks are visible at distinct q_z values. These peaks are partly obscured by the beamstop, but their finite extension along q_y—which is due to the correlated roughness of the lamellar interfaces[35]—allows us to identify their q_z-positions. For better statistics, we have integrated the scattered intensity along q_y

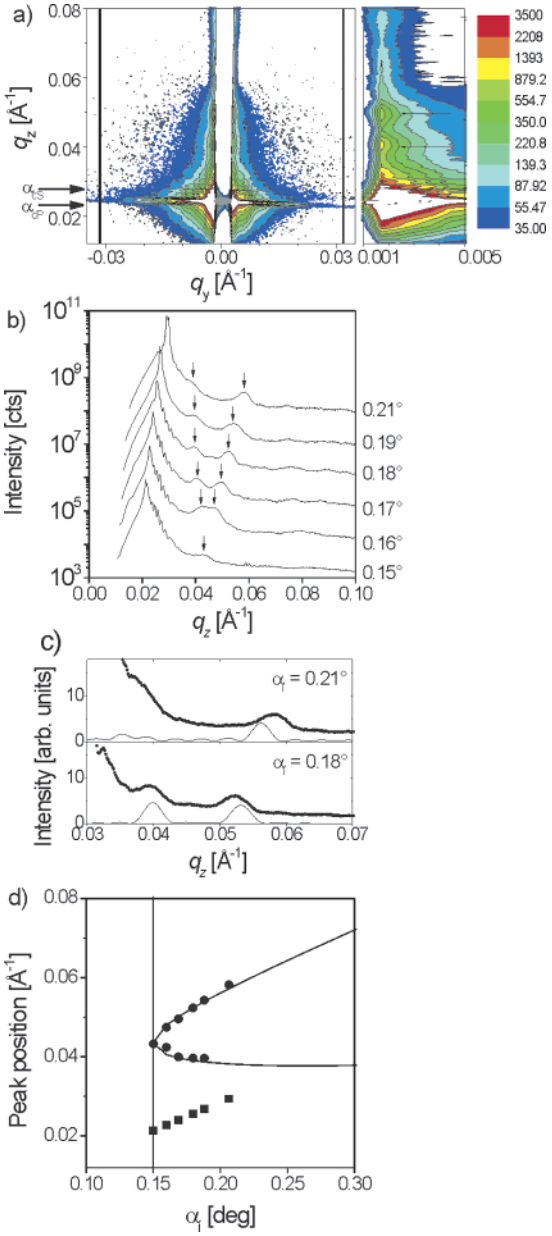

Figure 3. (a) GISAXS map ($\alpha_i = 0.17°$) of a film with block copolymer molar mass 22.6 kg/mol, $D^b_{lam} = 197$ Å and $D_{red} = 8.0$, together with an enlarged view of the region at low q_y (right panel). The measurement was performed at CHESS. In this and all other GISAXS maps, the intensity scale (in counts) is shown to the right. The vertical stripe of low intensity around $q_y = 0$ is caused by the beamstop which is necessary to protect the camera from the intense specularly reflected beam. The gray ellipse indicates the position of the specularly reflected beam; arrows on the left mark α_{cP} and α_{cS}. The vertical lines mark $q_y = \pm 2\pi/D^b_{lam}$. (b) Semilogarithmic representation of the intensity profiles along q_z for $q_y \cong 0$ (see Experimental Section) for different α_i (given to the right of each curve). The curves are shifted vertically for clarity. The arrows in (a) and (b) indicate the peaks attributed to the lamellar structure. (c) Experimental (●) intensity profiles and calculated ones (eq 22 in ref 22, lines). (d) q_z positions of the peaks in the curves in (b) as a function of α_i. (■) Specularly reflected beam; (●) additional diffuse peaks. Curved lines: fit of eq 1 with $m = 1$ (see text). The vertical line marks α_{cP}.

over the range $q_y = -0.005$ to 0.005 Å^{-1} (Figure 3b). The resulting curves are characterized by three main features: (i) The sharp peaks of high intensity are due to the shoulders of the specularly reflected beam, as given by the incident beam divergence and sample roughness. The Yoneda peaks of the polymer film and the substrate (expected at $\alpha_f = \alpha_{cP} = 0.15°$ and $\alpha_f = \alpha_{cS} = 0.22°$, respectively) overlap with the specularly

reflected beam because α_i lies between α_{cP} and α_{cS}. (ii) The short period oscillations on the high-q_z tail of the specularly reflected beam are probably caused by wave guide resonances or correlations of the film interfaces.[36] We refrain from a quantitative analysis because the maxima are very close to each other and reach the resolution limit of the setup. (iii) Additional peaks are present at $q_z \cong 0.04-0.06$ Å^{-1} which vary in a characteristic way with α_i. A comparison with the intensity profiles calculated for $q_{||} = 0$ with $D^f_{lam} = D^b_{lam}$ (eq 22 in ref 22, Figure 3c) shows that these peaks coincide with the calculated ones. For low α_i (0.18°), two first-order peaks (i.e., $m = 1$) are both predicted and observed. For higher α_i (0.21°), the peak at $q_z = 0.04°$ vanishes, in agreement with the calculated curve. D^f_{lam} and α_{cP} can be determined from a fit of eq 1 with $m = 1$, which leads to $D^f_{lam} = 199$ Å and $\alpha_{cP} = 0.150°$ (Figure 3d). These values are in excellent agreement with expectations. Thus, we conclude that the peaks are due to an internal lamellar structure where the lamellar interfaces are parallel to the film surface, and the lamellar thickness is very similar to the one in the bulk.

In order to compare the average number of correlated lamellae, N_c, in the film with D_{red}, we determine N_c from the fwhm of the Bragg peaks along q_z. For $\alpha_i = 0.18°$, the fwhm along q_z is 0.006 Å^{-1} for the peak at ~0.039 Å^{-1}. Note that the width of the specularly reflected beam along q_z, which reflects the resolution of our setup, only amounts to 0.001 Å^{-1}. N_c is given by[25]

$$N_c \approx \frac{2.75q^*}{\pi \times \text{fwhm}} \qquad (2)$$

with q^* being the peak position. N_c is obtained to be 5.3, which is of the same order as D_{red} (8.0). Thus, the prevalent lamellar orientation in this film is the parallel one over the entire, relatively large film thickness.

Thinner films of low molar mass P(S-*b*-B) show similar GISAXS maps. The map of a film from a polymer with the same molar mass (22.1 kg/mol) with $D_{red} = 2.4$ shows peaks at $q_y \cong 0$ near the positions expected from the DWBA prediction for 189 Å (Figure 4). Thus, the parallel orientation is confirmed also for this sample. However, the peaks are less pronounced and wider than for the thicker film, as expected. In addition, we observe some weak intensity in the GISAXS map at q_y values expected for perpendicular lamellae with $D^b_{lam} = 189$ Å (Figure 4a) indicative of the presence of perpendicular lamellae. The fwhm along q_y of these peaks is 0.019 Å^{-1} at the q_z value of the Yoneda peak, thus much larger than the fwhm of the specularly reflected beam of 0.003 Å^{-1}. Using eq 2, it is found that the domain size of the perpendicularly oriented lamellae corresponds to at most 2 times D^b_{lam}; i.e., the peaks are due to defects rather than to extended domains of perpendicularly oriented lamellae.

For a film of a block copolymer with 54.5 kg/mol and $D_{red} = 3.1$, terraces indicative of parallel lamellae close to the surface are present in the AFM images.[10] However, the terrace height of 302 Å was significantly smaller than $D^b_{lam} = 413$ Å. Figure 5a shows the two-dimensional GISAXS map of this film. The analysis of the vertical momentum transfer reveals only one pronounced peak for all incident angles (Figure 5b). The peaks expected near $q_z \cong 0.027$ Å^{-1} (Figure 5c), i.e., the term with the minus sign in eq 1 (which mainly arises from the term proportional to $J(\hat{q}_z,\hat{q}_z)$, see eq 22a in ref 22), probably overlap with the specularly reflected peak and the Yoneda peak of the substrate. Fitting the term with the plus sign and $m = 1$ in eq 1 to the peak positions (Figure 5c) leads to $D^f_{lam} = 380 \pm 12$ Å, i.e., again a value smaller than D^b_{lam}. Finally, a certain amount of unstructured scattering is visible in the 2D map. However, no Bragg rods are observed at the q_y-positions expected from perpendicular lamellae of a lamellar thickness of 413 Å (see vertical lines in Figure 5a). Thus, the main orientation of the lamellae in this film is parallel, in agreement with the terrace formation observed by AFM. Both the terrace height and the lamellar thickness in the film are reduced compared to the bulk lamellar thickness.

The AFM image of an ultrathin film with a film thickness slightly lower than D^b_{lam} (54.5 kg/mol and $D_{red} = 0.88$) is flat and homogeneous,[10] which is consistent with a single, slightly compressed lamella parallel to the film surface, i.e., $D^f_{lam} = D_{film}$. From this observation, we conclude that the same block wets both film surfaces; i.e., the boundary conditions are symmetric.[37] The GISAXS results confirm this structure (Figure

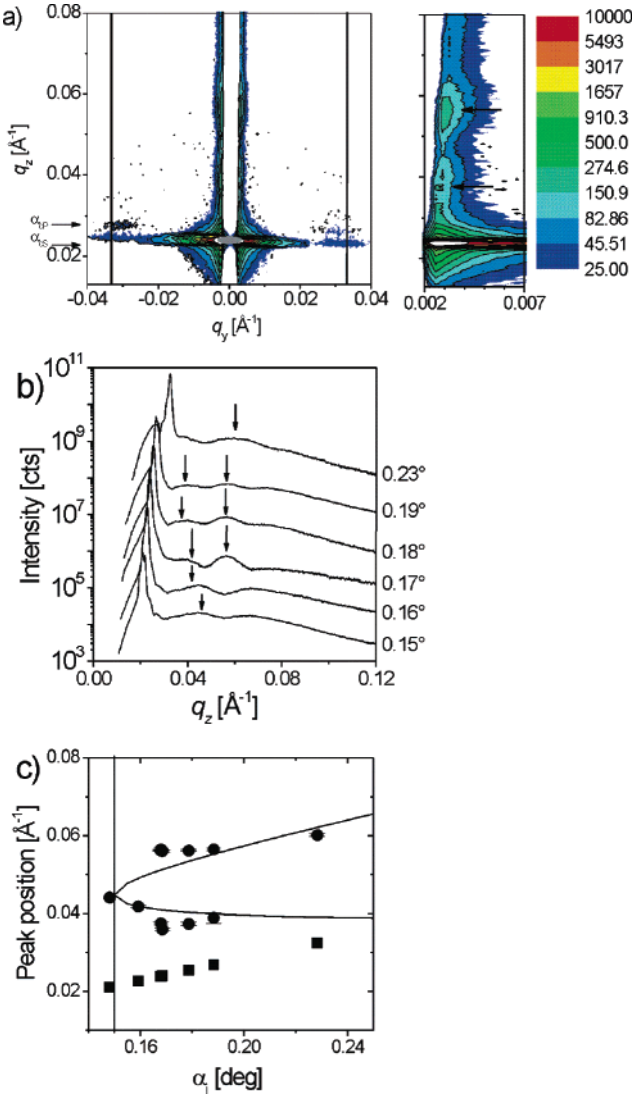

Figure 4. (a) GISAXS map ($\alpha_i = 0.17°$) of a film with block copolymer molar mass 22.1 kg/mol, $D^b_{lam} = 189$ Å, and $D_{red} = 2.4$. The measurement was performed at CHESS. The measuring time was 5 s. The vertical lines mark $q_y = \pm 2\pi/D^b_{lam}$. (b) Semilogarithmic representation of the intensity profiles along q_z for $q_y \cong 0$ (see Experimental Section) for different α_i (given to the right of each curve). The curves are shifted vertically for clarity. The arrows in (a) and (b) indicate the peaks attributed to the lamellar structure. (c) q_z positions of the peaks in the curves in (b) as a function of α_i. (■) Specularly reflected beam; (●) additional diffuse peaks. Curved lines: predictions from eq 1 with $m = 1$. The vertical line marks α_{cP}.

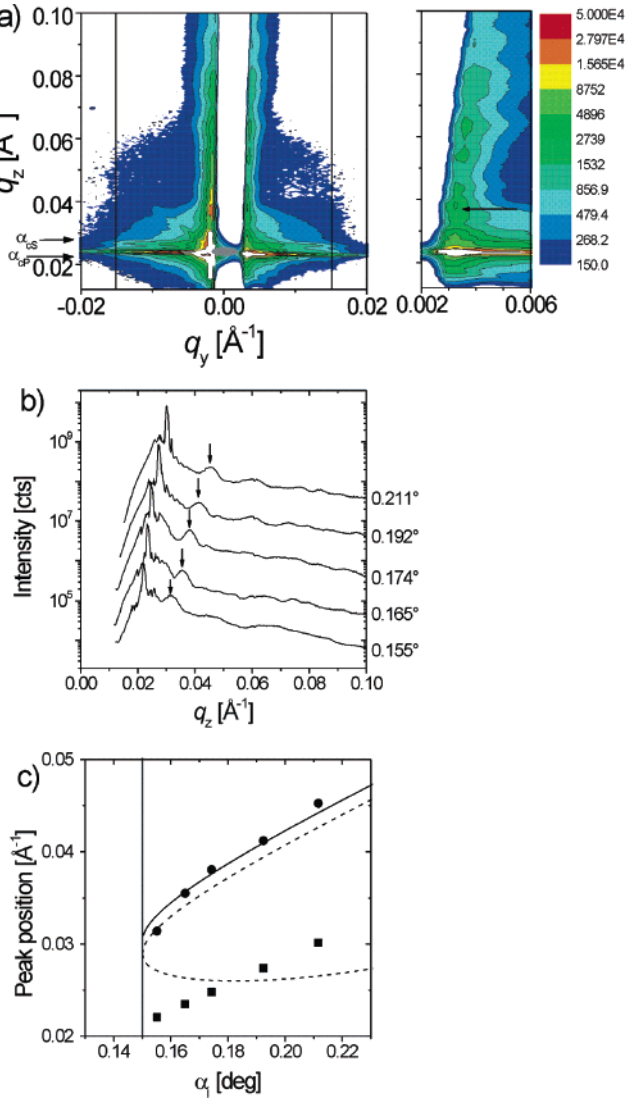

Figure 5. (a) GISAXS map of a sample with 54.4 kg/mol, D^b_{lam} = 413 Å, and D_{red} = 3.1, together with an enlarged view of the region at low q_y (right panel). α_i was 0.17°, and the exposure time was 50 s. The vertical lines mark $q_y = \pm 2\pi/D^b_{lam}$. The measurement was performed at CHESS. (b) Semilogarithmic representation of the intensity profiles along q_z for $q_y \cong 0$ (see Experimental Section) for different α_i (given to the right of each curve). The curves are shifted vertically for clarity. The arrows in (a) and (b) indicate the peaks attributed to the lamellar structure. (c) q_z positions of the peaks in the curves in (b) as a function of α_i. (■) Specularly reflected beam; (●) additional diffuse peaks. Curved dashed lines: predictions from eq 1 with $m = 1$ and D^f_{lam} = 413 Å; curved solid line: fit of eq 1 giving $D^f_{lam} = 380 \pm 12$ Å. The vertical line indicates α_{cP}.

6): No Bragg rods are observable, but weak peaks are observed in the intensity profiles along q_z which are in relatively good agreement with the predictions from eq 1 with $m = 1$ when D_{film} is used for D^f_{lam} (Figure 6c). The q_z widths of the peaks are 8.4×10^{-3}–2.5×10^{-2} Å^{-1} for the peaks at $q_z \cong 0.04$ Å^{-1}. Using eq 2, this leads to an average number of correlated lamellae of 1−4, which is in reasonable agreement with the D_{red} value of 0.88.

To conclude, the parallel lamellar orientation is found for thin films with molar mass below ~ 55 kg/mol and D_{red} in the range between 0.9 and 8. The lamellar thicknesses in the films correspond well with the ones known from the bulk.

Intermediate Molar Mass Regime. For a film of a block copolymer with molar mass 69.9 kg/mol and D_{red} = 3.2, the AFM image revealed a wavy surface topography, which is

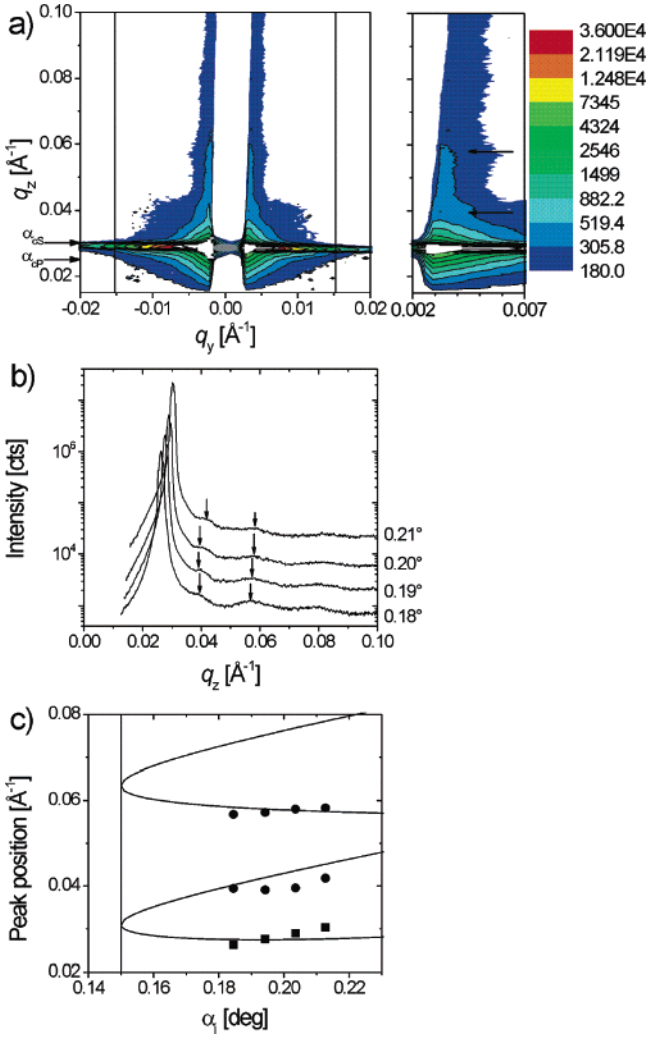

Figure 6. (a) GISAXS map of a sample with 54.4 kg/mol, D^b_{lam} = 413 Å, and D_{red} = 0.88. α_i was 0.20°, and the exposure time was 50 s. The vertical lines mark $q_y = \pm 2\pi/D^b_{lam}$. The measurement was performed at CHESS. (b) Semilogarithmic representation of the intensity profiles along q_z for $q_y \cong 0$ (see Experimental Section) for different α_i (given to the right of each curve). The curves are shifted vertically for clarity. The arrows in (a) and (b) indicate the peaks attributed to the lamellar structure. (c) q_z positions of the peaks in the curves in (b) as a function of α_i. (■) Specularly reflected beam; (●) additional diffuse peaks. Curved lines: predictions from eq 1 with $m = 1$, where D_{film} = 365 Å was used for D^f_{lam}. The vertical line indicates α_{cP}. The uncertainties of the q_z positions are similar to the symbol size.

different from terraces.[10] Neither could a lamellar surface pattern be found. The GISAXS map of this film (Figure 7a) shows a complex scattering pattern. At the q_y-position where the first-order Bragg rod would be expected ($2\pi/D^b_{lam} = 0.0136$ Å^{-1}), a clearly enhanced intensity is observed in the intensity profile at an exit angle close to α_{cP} (Figure 7b). Bragg rods are thus present, but they do not extend along q_z as expected for a perpendicular orientation of the lamellae throughout the entire film.[16] The vertical momentum transfers show a number of weak peaks (Figure 7c). We only evaluate the strongest one (Figure 7d), and a fit of eq 1 with $m = 1$ leads to $D^f_{lam} = 397 \pm 6$ Å, which is smaller than D^b_{lam} = 462 Å. The 2D map (Figure 7a) shows that the peaks along the q_z-axis are extended along q_y and bend downward, which can be attributed to a broad distribution of the lamellar normal vector centered around the surface normal, i.e., a partial powder ring. The partial ring may be related to the wavy appearance of the fim surface from the AFM image.

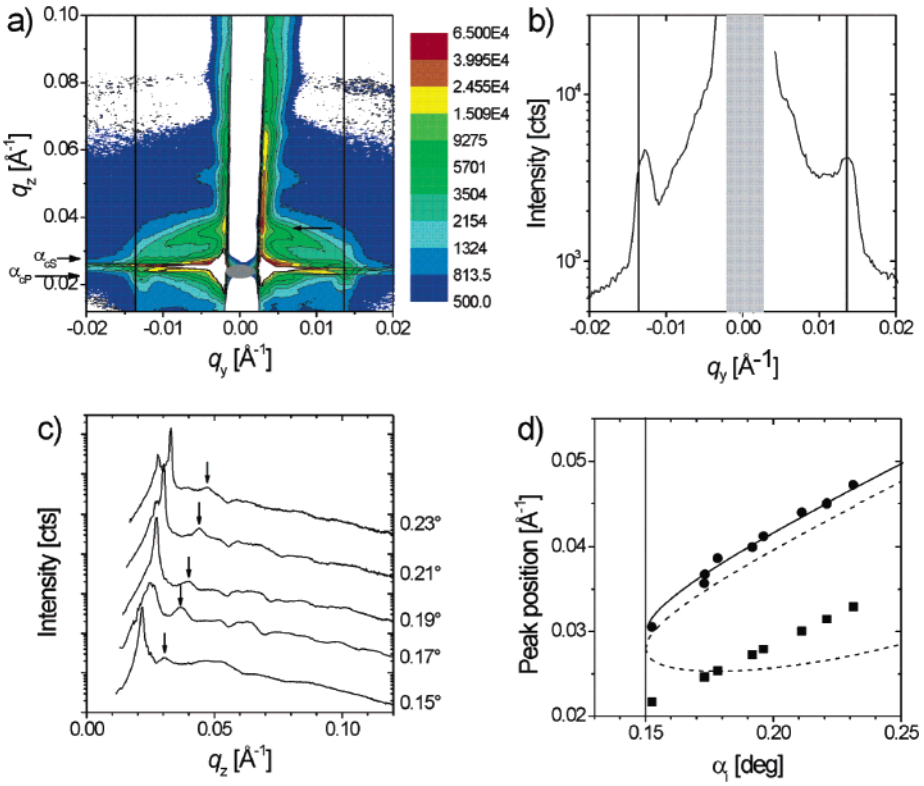

Figure 7. (a) GISAXS map of a sample with 69.9 kg/mol, D^b_{lam} = 462 Å, and D_{red} = 3.2. α_i was 0.17°. The exposure time was 100 s. The measurement was performed at CHESS. (b) Semilogarithmic representation of the intensity profile along q_y for q_z = 0.0230 Å^{-1} (the value corresponding to α_{cP}; see Experimental Section) for α_i = 0.17°. The vertical lines in (a) and (b) mark $q_y = \pm 2\pi/D^b_{lam}$. (c) Semilogarithmic representation of the intensity profiles along q_z for $q_y \cong 0$ (see Experimental Section) for different α_i (given to the right of each curve). The curves are shifted vertically for clarity. The arrows in (a) and (c) indicate the most important peak due to the lamellar structure. (d) q_z positions of the peaks in the curves in (c) as a function of α_i. (■) Specularly reflected beam; (●) additional diffuse peaks. Curved dashed lines: predictions from eq 1 with m = 1 and $D^f_{lam} = D^b_{lam}$; curved solid line: fit of eq 1 giving D^f_{lam} = 397 ± 6 Å. The vertical line indicates α_{cP}.

The GISAXS results of this film thus lead to the conclusion that the dominating orientation is the parallel one, with $D^f_{lam} \cong 0.86 D^b_{lam}$, and that the lamellar interfaces are wavy, as seen from the reflections along the film normal which are extended within the film plane. A fraction of the sample consists of perpendicular lamellae, giving rise to weak Bragg rods at the positions expected from D^b_{lam}. The GISAXS results together with the wavy film surface observed using AFM on the identical film are thus consistent with the coexistence of a range of different orientations of the lamellae, as suggested in our previous publication.[10]

High Molar Mass Regime. Films from block copolymer samples with molar masses of 148 and 183 kg/mol and reduced film thicknesses between two and three show a lamellar surface texture in tapping mode AFM, indicating a perpendicular orientation of the lamellae near the surface.[10] A thick film with a molar mass of 183 kg/mol shows a surface pattern with a dominating length scale of the order of D^b_{lam}; however, in contrast to the thinner films, the correlation length is rather low.[10] GISAXS allowed us to investigate whether the lamellae are perpendicular throughout the entire film thickness in the same way as for the relatively thin films or whether other orientations are present.

Figure 8 shows a GISAXS map of a film with a reduced thicknesses of D_{red} = 4.4 and a molar mass of 183 kg/mol. Bragg rods, which are elongated along q_z, are located at $q_y = (7.03 \pm 0.34) \times 10^{-3}$ Å^{-1}; see also the peaks in the intensity profile along q_y taken at q_z = 0.043 Å^{-1} (Figure 8b). The corresponding repeat distance is $2\pi/q_y$ = 894 ± 43 Å, which is, within the uncertainties, identical to the bulk lamellar thickness (839 ± 13 Å) and to the repeat distance found using AFM (855 ± 4 Å).[10] The Bragg rods have maximum intensity at q_z values corresponding to $\alpha_f = \alpha_{cS}$ and α_{cP}, which is due to the Yoneda effect, consistent with the DWBA model.[22] We conclude that the perpendicular orientation observed at the film surface prevails throughout the entire film thickness. In the GISAXS map, a weak second-order Bragg reflection is observed, which points to a slight asymmetry of the lamellae. The third order is absent, which is indicative of limited long-range order in the films. AFM images indicate that the perpendicular lamellae stacks form meandering structures of a domain size not much larger than a few lamellar thicknesses. This is confirmed by the peak width along q_y, which leads to $N_c \geq 2$.

In contrast, a thicker film (183 kg/mol, D_{red} = 8.8) indicates the transition to the bulk limit, i.e., random lamellar orientation due to a loss of the orienting influence of the air−polymer and the polymer−substrate interface. The AFM image of this film shows a textured surface with a dominating wavelength comparable to D^b_{lam}.[10] The GISAXS maps reveal the inner film structure in great detail, achieving a certain degree of depth sensitivity by using different α_i: In the GISAXS map taken at α_i = 0.13° (Figure 9a), the scattering arises only from a thin layer of ~50 Å below the film surface because $\alpha_i < \alpha_{cP}$.[38] Two Bragg rods at q_y-positions corresponding to repeat distances of 836 ± 17 Å are present, which is in very good agreement with the bulk value D^b_{lam} = 839 ± 13 Å.[25] Thus, GISAXS in evanescent wave conditions reveals that the lamellae are perpendicular to the film surface in a thin layer below the surface. The lamellar structure *inside* the film is probed in GISAXS measurements with $\alpha_i > \alpha_{cP}$, where the scattered

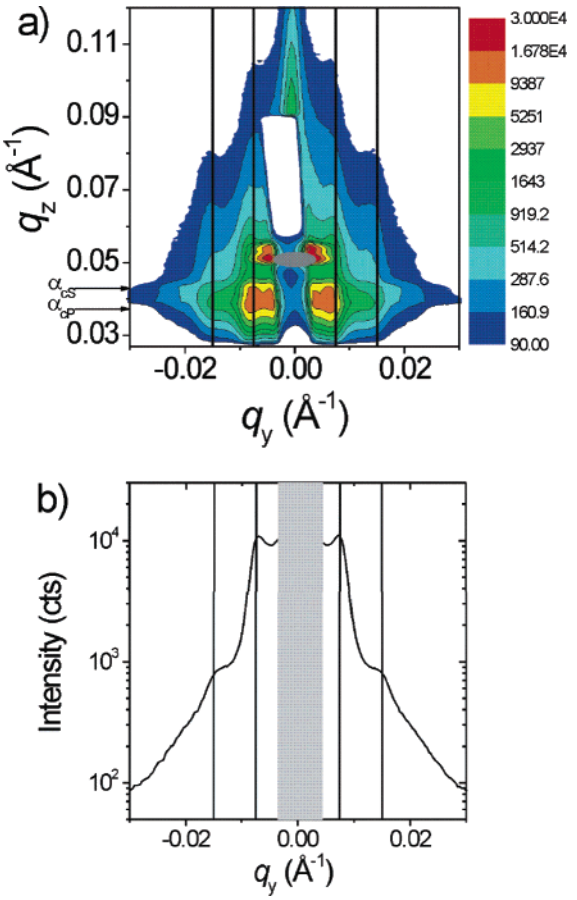

Figure 8. (a) GISAXS map of a film with $\bar{M}_n = 183$ kg/mol, $D^b_{lam} = 839$ Å, $D_{red} = 4.4$, and $\alpha_i = 0.32°$. The exposure time was 2000 s. The measurement was performed at HASYLAB. (b) Semilogarithmic representation of the intensity profile along q_y from the GISAXS map in (a), taken at $q_z = 0.043$ Å^{-1}, corresponding to the row of highest intensity. The q_z width of the cut is 9.72×10^{-4} Å^{-1}. The gray region in the center indicates the beamstop. The vertical lines in (a) and (b) indicate $q_y = 2\pi/D^b_{lam}$ and $4\pi/D^b_{lam}$.

intensity stems from the entire film (Figure 9b,c). In both images, in addition to the Bragg rods, a ring of high intensity centered at the specularly reflected peak is observed. Such a ring is due to lamellae having a distribution of tilt angles. When α_i is increased, the ring moves along with the specularly reflected beam toward higher q_z. We conclude that, near the film surface, the lamellae are perpendicular, consistent with the AFM results reported earlier.[10] Inside the film, perpendicular lamellae coexist with randomly oriented ones. The lateral radius of the ring coincides with the Bragg rods; its radius is thus equal to the momentum transfer q_y of the Bragg rods, independent of α_i. The radius along q_z follows eq 1 using the bulk D^b_{lam} and $m = 1$; i.e., refraction of the X-ray wave has to be taken properly into account (not shown).

In summary, in the high molar mass film having $D_{red} = 4.4$, the perpendicular orientation is predominant, and no other orientations could be detected using GISAXS. The same holds for $D_{red} = 2.6$.[20] The transition from the (expected) parallel orientation to the perpendicular orientation by variation of the molar mass is an unexpected finding, and possible reasons will be discussed below. For $D_{red} = 8.8$ (and probably above), other lamellar orientations are present in significant amounts. The preferential ordering induced by the film/substrate and film/air interfaces thus seems to get lost between $D_{red} = 4.4$ and 8.8. The lamellar thicknesses in the film are similar to the ones in the bulk.

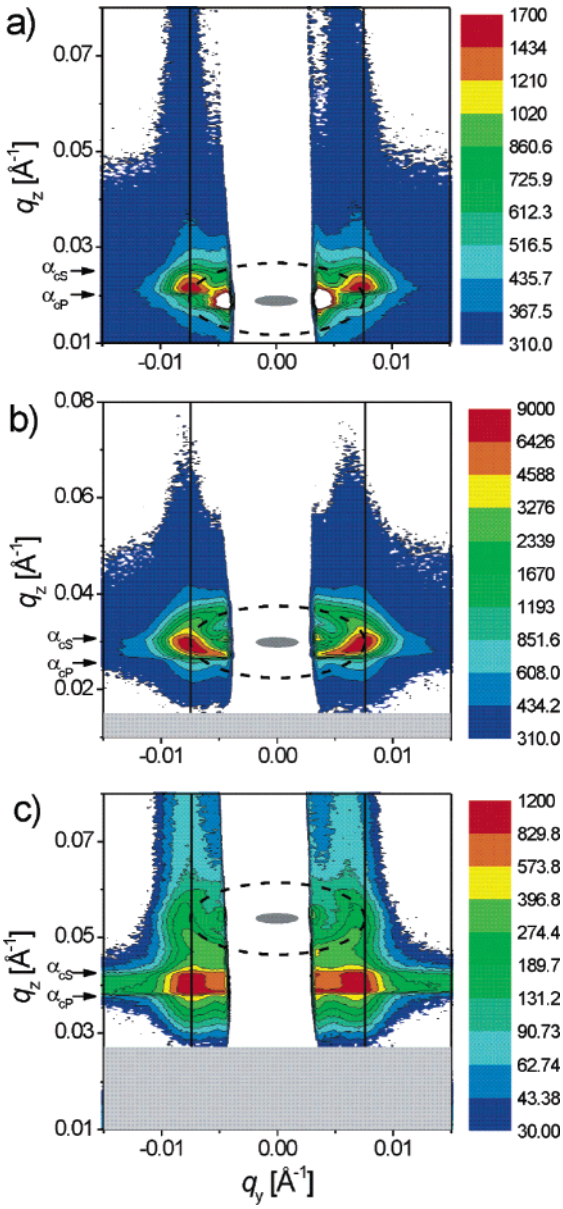

Figure 9. GISAXS maps of a film with $\bar{M}_n = 183$ kg/mol, $D^b_{lam} = 839$ Å, and $D_{red} = 8.8$ taken at incident angles of (a) 0.13°, (b) 0.21°, and (c) 0.38°. The measurement was performed at ESRF. In the gray regions in the bottom parts of (b) and (c), the detected intensity is obstructed by the sample itself. The vertical lines indicate $q_y = 2\pi/D^b_{lam}$. The dashed ellipses represent circles in (q_y, q_z)-space having radii of 7.49×10^{-3} Å^{-1}.

Discussion

Before discussing the findings, we will briefly summarize the benefit of the GISAXS technique as a tool to study the structure in the interior of the film.

The GISAXS Technique. GISAXS allows a quantitative determination of the lamellar structure inside the block copolymer films. It has proven to be useful to carry out measurements of the 2D maps at several incident angles around the critical angles of the polymer film and the substrate in order to gain depth sensitivity and to benefit from the enhanced intensity between α_{cP} and α_{cS}. Because of this enhancement, the measuring times are short—much shorter than in a convential X-ray reflectometry experiment, for instance. The dynamic effects can be taken into account by a DWBA model.[22] In this way, we were, on the one hand, able to prove that peaks along the film normal are due to lamellae which have the parallel

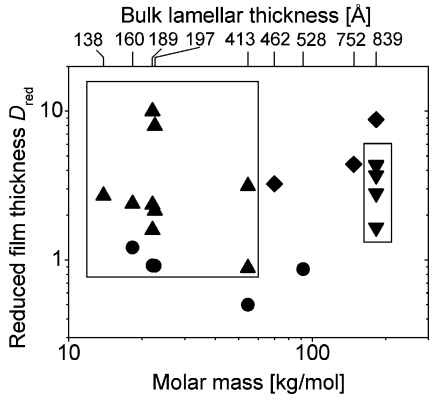

Figure 10. Orientation diagram of the lamellar orientation in the film as observed using GISAXS. The orientations are given as a function of block copolymer molar mass (bottom axis) or bulk lamellar thickness (top axis, values from ref 25) and of the reduced film thickness. Triangles up: parallel; triangles down: perpendicular; diamonds: coexisting orientations; circles: no scattering observed.

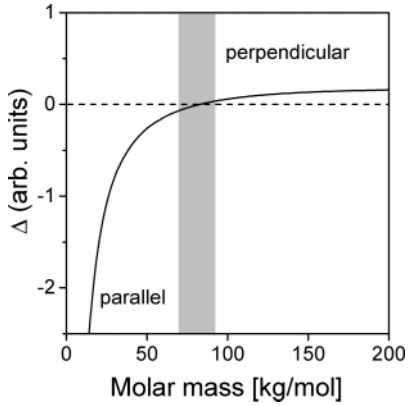

Figure 11. Difference of the free energies associated with the parallel and the perpendicular orientation, Δ, calculated using eq 3 (rewritten from ref 5) with the following coefficients: $c_w = 0$, $c_n = 0.2$, $c_e = 1$. The horizontal dashed line marks the transition between the regions of stability of the parallel (negative values of Δ) and the perpendicular orientation (positive values). The gray region marks the molar mass region where the transition from the parallel to the perpendicular orientation is observed in our experiments. At the transition, the energy differences between the lamellar orientations are small; hence, the observed coexistence of different lamellar orientations could be due to kinetic limitations.

orientation inside the films, and we could determine the lamellar thickness in the films (Figures 3−6). The perpendicular orientation, on the other hand, is characterized by elongated Bragg rods at q_y positions equal to $2\pi/D^b_{lam}$ (and multiples thereof, Figure 8). The intensity profiles of the Bragg rods along q_z show maxima near α_{cP} and α_{cS}, which can be understood when taking dynamic effects into account. Coexistence of several lamellar orientations could be detected for a few samples (Figures 7 and 9).

The Orientation Diagram. The lamellar orientations found in the GISAXS experiments described above are compiled in Figure 10 as a function of the reduced film thickness D_{red} (left axis) and the block copolymer molar mass (bottom axis). The bulk lamellar thicknesses measured by SAXS and SANS[25] are given on the top axis. For low molar mass samples ($\bar{M}_n \leq 54.5$ kg/mol) with $D_{red} = 1.6-3.3$, the GISAXS maps confirm the parallel orientation deduced from the AFM experiments (Figures 2−5).[10] The GISAXS maps of an ultrathin film ($D_{red} = 0.88$, Figure 6) showed the parallel orientation as well, which is consistent with symmetric wetting. The lamellar thickness is decreased and is equal to the film thickness. A few other ultrathin films ($D_{red} \leq 1.2$) did not show any scattering, presumably because there is too little polymer material on the substrate. Thick, low molar mass films ($D_{red} = 8.0$ and 10, e.g., Figure 3) show exclusively the parallel orientation. The parallel orientation is indeed expected, if we take only the difference of the interfacial interactions of the PS and the PB blocks with the SiO_x substrate together with the difference in surface tensions of the two blocks into account. PB has a lower surface tension than PS and will therefore form the top layer of the film. Our AFM experiments on ultrathin films have shown that the same block (i.e., PB) wets both the film surface and the film/substrate interface.[10] The parallel orientation has been observed frequently in thin, supported films of chemically different systems, such as poly(styrene-*b*-methyl methacrylate) (P(S-*b*-MMA)) or poly(styrene-*b*-butyl methacrylate) (P(S-*b*-BMA)).[30−34,39−42]

However, for higher molar masses, other lamellar orientations are observed: For a sample with 69.9 kg/mol, wavy parallel lamellae coexist with perpendicular lamellae (Figure 7). For high molar mass films (183 kg/mol and $D_{red} = 1.6-4.4$), the lamellae are perpendicular with the same lamellar thickness as in the bulk, which is consistent with our AFM results (Figure 8).[10] Only for higher D_{red} values, the stabilizing influence of the film interfaces is lost, and the perpendicular orientation coexists with domains of random orientation (Figure 9). Thus, between $D_{red} = 4.4$ and 8.8, the orienting influence of the air/polymer and the polymer/substrate interfaces is gradually lost. In the bulk, we have found that for annealed samples with 183 kg/mol approximately seven lamellae are correlated in orientation.[25] It seems that films having $D_{red} > \sim 7$ approach the bulk limit of randomly oriented lamellar domains.

Mechanism of Structure Formation. The majority of theoretical approaches and of numerical simulations deals with thin block copolymer films between two hard walls[9,43−47] and thus do not directly apply to our situation of thin, supported block copolymer films. In a few publications, however, possible explanations have been put forward for the transition from parallel to perpendicular orientation upon varying the block copolymer molar mass in thin, supported P(S-*b*-B) films.

(i) The most simple thermodynamic approach involves only the selectivity of the air−polymer and the polymer−substrate interfaces, i.e., the difference in the surface tensions of PS and PB and of the interfacial tensions of PS and PB toward the SiO_x substrate. The influence of the substrate selectivity on the adjacent lamellar orientation has been demonstrated for thin films of P(S-*b*-MMA) by using selective and nonselective substrates, leading to the purely parallel and the purely perpendicular orientation, respectively.[48,49] We note that even for the nonselective substrate only the perpendicular orientation is present and not a random orientation, which might be expected for a purely neutral surface. This suggests the contribution of additional terms, most probably entropic in nature. Pickett et al. have included additional, entropic terms into a description of the interaction of a lamellar block copolymer melt with a hard wall.[5] These terms are molar mass dependent and comprise the enrichment of chain ends near a hard wall and the stretching of copolymers along a hard wall. The difference of free energies between the parallel and the perpendicular orientation, Δ, is expressed as a function of these two terms in addition to the free energy related to the wall selectivity:

$$\Delta \propto -c_w + c_n M^{-2/3} - c_e M^{-8/9} \qquad (3)$$

M denotes the overall block copolymer molar mass, and the c coefficients describe the strengths of the enthalpic (wetting term c_w) and the two entropic terms (nematic term c_n and chain

end effects c_e). In our P(S-*b*-B) system, the selectivities of the film interfaces are presumably low: The difference of surface tensions is 5 mN/m, which amounts to 16%. The interfacial tensions of PS and PB toward SiO_x are not known, but one can assume that the difference is small because both blocks are rather nonpolar, in contrast to SiO_x. Assuming that the selectivity term is negligible (we choose here for simplicity $c_w = 0$), a set of coefficients can be found for the two entropic terms ($c_e = 1$ and $c_n = 0.2$) which reproduces the observed transition of lamellar orientation observed in P(S-*b*-B) on SiO_x at a molar mass between 69.9 and 91.9 kg/mol (Figure 11). A quantitative application of the model is not possible because not all c parameters in the model have been expressed in terms of material parameters.[5] The perpendicular lamellar orientation close to a nonselective wall has been found in numerical simulations as well and has been attributed to entropic effects.[6] If this model applies to explain the perpendicular orientation in P(S-*b*-B) on SiO_x, it can be concluded that the perpendicular orientation formed near the hard wall (i.e., the substrate) persists along the film normal over a few D_{lam}^{b}, such that the purely perpendicular orientation is obtained up to $D_{red} = 4.4$, but not for $D_{red} = 8.8$. It is also possible that the perpendicular lamellar orientation is induced at the air−polymer interface and spreads to the substrate. Finally, both interfaces may induce the same ordering. On the basis of our present data, we cannot make a statement about which interface is responsible. However, the evanescent wave data from the thick, high molar mass film (Figure 9a) indicate that ordering may start from the film surface.

(ii) Thin supported films have been described recently in the strong-segregation limit.[7] The parallel orientation was generally predicted for the thin film geometry; however, perpendicular lamellae were found to be stable even for thick films when the spreading parameters of both blocks are close to each other or, for thin enough films with dissimilar spreading parameters, stability of the perpendicular orientation is found under wetting conditions for both blocks. However, a comparison to our data shows that the model does not reproduce the transition of the lamellar orientation in the P(S-*b*-B) system with molar mass. A possible reason may be that not all our samples are in the strong-segregation regime, only the ones with molar masses $\geq$54.5 kg/mol. (The χ parameter at room temperature differs only by ~30% from the one at 150 °C, so the transition is only shifted by a small factor.) The samples with lower molar masses are in the bulk in the intermediate-segregation regime.[24] Work on the influence of the segregation on the orientational behavior in thin film geometry is in progress.[50]

In summary, we have confirmed our previous AFM observations[10] that the orientation of symmetric diblock copolymers of P(S-*b*-B) in thin films depends strongly on molar mass. The GISAXS measurements provide additional details on the internal ordering within the films. For many other symmetric diblock copolymer systems, the parallel orientation has nearly always been observed for selective surfaces. Thus, for these systems, the orientation is stabilized by the difference in interfacial tensions of the two blocks with respect to the film interfaces. However, our findings show that in the case of P(S-*b*-B) also the perpendicular orientation can be formed, provided the molar mass is high enough. Even though we cannot conclusively explain the origin of this behavior, we suggest that entropic contributions play an important role for the orientation of the lamellae.

Acknowledgment. We thank B. Rheinländer, Universität Leipzig, for ellipsometry measurements, O. Konovalov, ESRF, for assistance at ESRF beamline ID10B, E. Fontes for help at CHESS D-line, S. V. Roth, HASYLAB, and P. Michelberger, TU München, for help at BW4 at HASYLAB/DESY, and I. I. Potemkin, Moscow State University, for stimulating discussions. We thank the European Synchrotron Radiation Facility (ESRF), the Cornell High-Energy Synchrotron Source (CHESS), and HASYLAB for providing us with high-intensity X-ray beams and high-quality instrumentation. CHESS is a national user facility supported by the National Science Foundation and the National Institutes of Health/National Institute of General Medical Sciences under Award DMR-0225180. Financial support by Deutsche Forschungsgemeinschaft (Pa 771/1-1), NATO, DANSYNC, and Fonds der Chemischen Industrie is gratefully acknowledged. D.P. acknowledges the never failing support and encouragement given to her by Lasse Holst Sørensen.

References and Notes

(1) Hamley, I. W. *Nanotechnology* **2003**, *14*, R39.
(2) Lazzari, M.; Lopez-Quintela, M. A. *Adv. Mater.* **2003**, *15*, 1583.
(3) Granick, S.; et al. *J. Polym. Sci., Part B: Polym. Phys.* **2003**, *41*, 2755.
(4) Du, P.; Li, M.; Douki, K.; Li, X.; Garcia, C. B. W.; Jain, A.; Smilgies, D.-M.; Fetters, L. J.; Gruner, S. M.; Wiesner, U.; Ober, C. K. *Adv. Mater.* **2004**, *16*, 953.
(5) Pickett, G. T.; Witten, T. A.; Nagel. S. R. *Macromolecules* **1993**, *26*, 3194.
(6) Sommer, J.-U.; Hoffmann, A.; Blumen, A. *J. Chem. Phys.* **1999**, *111*, 3278.
(7) Potemkin, I. I. *Macromolecules* **2004**, *37*, 3505.
(8) Tsori, Y.; Sivaniah, E.; Andelman, D.; Hashimoto, T. *Macromolecules* **2005**, *38*, 7193.
(9) Geisinger, T.; Müller, M.; Binder, K. *J. Chem. Phys.* **1999**, *111*, 5241 and 5251.
(10) Busch, P.; Posselt, D.; Smilgies, D.-M.; Rheinländer, B.; Kremer, F.; Papadakis, C. M. *Macromolecules* **2003**, *36*, 8717; **2006**, *39*, 3098 (erratum).
(11) Müller-Buschbaum, P.; Wolkenhauer, M.; Wunnicke, O.; Stamm, M.; Cubitt, R.; Petry, W. *Langmuir* **2001**, *17*, 5567.
(12) Müller-Buschbaum, P.; Cubitt, R.; Petry, W. *Langmuir* **2003**, *19*, 7778.
(13) Müller-Buschbaum, P.; Gutmann, J. S.; Lorenz-Haas, C.; Mahltig, B.; Stamm, M.; Petry, W. *Macromolecules* **2001**, *34*, 7463.
(14) Müller-Buschbaum, P.; Gutmann, J. S.; Lorenz-Haas, C.; Wunnicke, O.; Stamm, M.; Petry, W. *Macromolecules* **2002**, *35*, 2017.
(15) Müller-Buschbaum, P.; Hermsdorf, N.; Roth, S. V.; Wiedersich, J.; Cunis, S.; Gehrke, R. *Spectrochim. Acta, Part B* **2004**, *59*, 1789.
(16) Smilgies, D.-M.; Busch, P.; Papadakis, C. M.; Posselt, D. *Synchrotron Radiat. News* **2002**, *15*, 35.
(17) Kim, S. H.; Misner, M. J.; Xu, T.; Kimura, M.; Russell, T. P. *Adv. Mater.* **2004**, *16*, 226.
(18) Li, M.; Douki, K.; Goto, K.; Li, X.; Coenjarts, C.; Smilgies, D.-M.; Ober, C. K. *Chem. Mater.* **2004**, *16*, 3800.
(19) Lee, B.; Park, I.; Yoon, J.; Park, S.; Kim, J.; Kim, K.; Chang, T.; Ree, M. *Macromolecules* **2005**, *38*, 4311.
(20) Papadakis, C. M.; Busch, P.; Posselt, D.; Smilgies, D.-M. *Adv. Solid State Phys.* **2004**, *44*, 327.
(21) Xu, T.; Hawker, C. J.; Russell, T. P. *Macromolecules* **2005**, *38*, 2802.
(22) Busch, P.; Rauscher, M.; Smilgies, D.-M.; Posselt, D.; Papadakis, C. M. *J. Appl. Crystallogr.* **2006**, *39*, 433.
(23) Ndoni, S.; Papadakis, C. M.; Bates, F. S.; Almdal, K. *Rev. Sci. Instrum.* **1995**, *66*, 1090.
(24) Papadakis, C. M.; Almdal, K.; Mortensen, K.; Posselt, D. *Europhys. Lett.* **1996**, *36*, 289.
(25) Papadakis, C. M.; Almdal, K.; Mortensen, K.; Posselt, D. *J. Phys. II* **1997**, *7*, 1829.
(26) Rudd, J. F. In *Polymer Handbook*, 2nd ed.; Brandrup, J., Immergut, E. H., Eds.; Wiley: New York, 1989.
(27) Turturro, A.; Gattiglia, E.; Vacca, P.; Viola, G. T. *Polymer* **1995**, *36*, 3987.
(28) Gruner, S. M.; Tate, M. W.; Eikenberry, E. F. *Rev. Sci. Instrum.* **2002**, *73*, 2815.
(29) Tolan, M. *X-Ray Scattering from Soft-Matter Thin Films*; Springer: Berlin, 1999; p 7.
(30) Ausserré, D.; Chatenay, D.; Coulon, G.; Collin, B. *J. Phys. (Paris)* **1990**, *51*, 2571.
(31) Coulon, G.; Collin, B.; Ausserré, D.; Chatenay, D.; Russell, T. P. *J. Phys. (Paris)* **1990**, *51*, 2801.
(32) Maaloum, M.; Ausserré, D.; Chatenay, D.; Coulon, G.; Gallot, Y. *Phys. Rev. Lett.* **1992**, *68*, 1575.

(33) Cai, Z. H.; Huang, K.; Montano, P. A.; Russell, T. P.; Bai, J. M.; Zajak, G. W. *J. Chem. Phys.* **1993**, *98*, 2376.
(34) Cai, Z. H.; Lai, B.; Yun, W. B.; McNulty, I.; Huang, K. G.; Russell, T. P. *Phys. Rev. Lett.* **1994**, *73*, 82.
(35) Gutmann, J. S.; Müller-Buschbaum, P.; Schubert, D. W.; Stribeck, N.; Smilgies, D.; Stamm, M. *Physica B* **2000**, *283*, 40.
(36) Müller-Buschbaum, P.; Stamm, M. *Macromolecules* **1998**, *31*, 3686.
(37) Fasolka, M. J.; Mayes, A. M. *Annu. Rev. Mater. Res.* **2001**, *31*, 323.
(38) Als-Nielsen, J.; McMorrow, D. *Elements of Modern X-Ray Physics*; John Wiley & Sons Ltd.: Chichester, 2001.
(39) Anastasiadis, S. H.; Russell, T. P.; Satija, S. K.; Majkrzak, C. F. *Phys. Rev. Lett.* **1989**, *62*, 1852.
(40) Coulon, G.; Ausserré, D.; Russell, T. P. *J. Phys. (Paris*) **1990**, *51*, 777.
(41) Mansky, P.; Russell, T. P.; Hawker, C. J.; Mays, J.; Cook, D. C.; Satija, S. K. *Phys. Rev. Lett.* **1997**, *79*, 237.
(42) Mansky, P.; Russell, T. P.; Hawker, C. J.; Pitsikalis, M.; Mays, J. *Macromolecules* **1997**, *30*, 6810.
(43) Turner, M. S. *Phys. Rev. Lett.* **1992**, *69*, 1788.
(44) Walton, D. G.; Kellogg, G. J.; Mayes, A. M.; Lambooy, P.; Russell, T. P. *Macromolecules* **1994**, *27*, 6225.
(45) Matsen, M. W. *J. Chem. Phys.* **1997**, *106*, 7781.
(46) Tang, W. H.; Witten, T. A. *Macromolecules* **1998**, *31*, 3130.
(47) Tsori, Y.; Andelman, D. *Eur. Phys. J. E* **2001**, *5*, 605.
(48) Mansky, P.; Russell, T. P.; Hawker, C. J.; Pitsikalis, M.; Mays, J. *Macromolecules* **1997**, *30*, 6810.
(49) Huang, E.; Mansky, P.; Russell, T. P.; Harrison, C.; Chaikin, P. M.; Register, R. A.; Hawker, C. J.; Mays, J. *Macromolecules* **2000**, *33*, 80.
(50) Potemkin, I. I.; Busch, P.; Smilgies, D.-M.; Posselt, D.; Papadakis, C. M. *Macromol. Rapid Commun.*, in press.

MA061695C